Cooperative Effect of Molecular Orientation and β-Form on Toughening Injection-Molded Isotactic Polypropylene with β-Nucleating Agent

Ruihua Lv, Zhujun Li, Bing Na, Shufen Zou, Huayan Pan

Fundamental Science on Radioactive Geology and Exploration Technology Laboratory, School of Biology, Chemistry and Material Science, East China Institute of Technology, Fuzhou 344000, People's Republic of China

Received 25 July 2011; accepted 5 December 2011
DOI 10.1002/app.36622
Published online 30 January 2012 in Wiley Online Library (wileyonlinelibrary.com).

ABSTRACT: The toughness of conventional injection-molded isotactic polypropylene bars has been investigated with respect to the notch location and β-nucleating agent. Superior toughness is achieved in the β-nucleated bars with notches near the gate, but is absent in the near-gate bars without β-nucleating agent or in the β-nucleated ones far from the gate. With detailed structural analysis across the sample thickness, it is indicated that in these tough bars, extensive flow close to the surface suppresses the formation of β-form to a large extent but favors the generation of oriented α-form, whereas toward inner region, an opposite tendency is presented with the decay of flow strength and the activation of β-nucleating agent. Allowing that this peculiar hierarchical structure is absent in other two kinds of bars, it is deduced that the cooperative effect of molecular orientation of α-form in the skin layer and rich β-form in the inner region is responsible for the significant toughness enhancement in the β-nucleated bars near the gate. © 2012 Wiley Periodicals, Inc. J Appl Polym Sci 125: 2764–2770, 2012

Key words: molecular orientation; **β**-form; isotactic polypropylene

INTRODUCTION

In the past decades, the study on the β-form of isotactic polypropylene (iPP) has attracted extensive attention because of its superior toughness to α-form.[1–10] As a metastable crystal modification, it is rare for the occurrence of β-form under normal processing conditions. In contrast, β-form is readily produced through crystallization of iPP in the temperature gradient,[11,12] under flow,[13–15] or in the presence of specific β-nucleating agent.[1–10] Of them, adding β-nucleating agent is an effective and popular routine to obtain high level of β-form. It has been well demonstrated that the formation of β-form in a β-nucleated iPP under quiescent conditions is affected by several factors, such as crystallization temperature, final melting temperature, molecular architecture of iPP, and the content of β-nucleating agent.[8,15–18]

As flow is inevitably involved in fabricating final products through practical processing methods, e.g., injection molding, the understanding of crystallization of β-nucleated iPP under flow conditions is another pursuit.[19–22] Although individual flow or β-nucleating agent can induce β-form during crystallization of iPP, combination of them does not mean the synergistic effect in producing high concentration β-form. What is worse, at high flow rate, the formation of β-form in iPP with β-nucleating agent is completely suppressed and only α-form is presented,[21,22] as a result of favorable α-nucleation induced by flow.

Even so, combination of flow and β-nucleating agent seems an alternative to tailor the microstructure and mechanical properties of iPP in practical processing where flow gradient is endured. It has been claimed that bamboo-like structure, with highly oriented α-form and dominant β-form spherulites in the outer and core layer, respectively, is generated in the injection-molded β-nucleated iPP parts[21,22]; it, in turn, results in simultaneous enhancement of strength (contributed by the oriented α-form in the outer layer) and toughness (originated from the rich β-form in the core layer). Of note, in these studies, special injection molding methods, namely, oscillation shear injection molding or dynamic packing injection molding, were adopted; and highly oriented

Correspondence to: B. Na (bingnash@163.com; bna@ecit.edu.cn).

Contract grant sponsor: National Natural Science Foundation of China; contract grant number: 20704006.
Contract grant sponsor: Project of Jiangxi Provincial Department of Education; contract grant numbers: GJJ08295 and GJJ11138.
Contract grant sponsor: State Key Laboratory of Polymer Materials Engineering (Opening Project), Sichuan University.

layer almost penetrated the whole cross section of molded parts. However, as a widely used polymer-processing approach, conventional injection molding can only endow thin oriented layers close to the wall of a cold mold,[23–26] which has little influence on the mechanical properties of molded iPP parts. Hence, one may wonder if combination of flow and β-nucleating agent can impart superior mechanical properties to the conventional injection-molded parts.

To clarify this, the hierarchical structure and related mechanical properties of conventional injection-molded iPP bars with respect to the notch location and β-nucleating agent have been explored. It is indicated that remarkable toughness enhancement was indeed achieved in the β-nucleated iPP bars with notches near the gate, arising from the cooperative effect of molecular orientation of α-form in the skin layer and rich β-form in the inner region.

EXPERIMENTAL

Material and sample preparation

A commercially available iPP, purchased from Dushanzi Petrochemical, China, was used. It had a melt flow rate of 2.5 g/10 min and a nominal melting point of about 165°C, respectively. The rare earth β-nucleating agent, marked as WBG-II, was supplied by Winner Functional Materials (Foshan, Guangdong, China). The master batch of iPP with 5 wt % WBG were first prepared in a twin-screw extruder with the barrel temperature of 160–200°C; then, the master batch was diluted by adding pure iPP to prepare pellets containing 0.1 wt % WBG. For comparison, pure iPP was also subjected to the same processing procedures. Rectangle bars (4.2 mm thickness × 10.2 mm width × 150 mm length) were prepared using a conventional screw-type injection molding machine with the barrel and mold temperature of 200 and 30°C, respectively.

Two-dimensional wide angle X-ray diffraction

Two-dimensional wide angle X-ray diffraction (2D-WAXD) measurements were conducted on the diffraction workstation in the National Synchrotron Radiation Laboratory, Hefei, China. The wavelength of X-ray was 0.154 nm, and the transmission mode was used. A series of 0.2-mm thick slices were cut from the molded bars, located at 35 mm away from two ends, respectively, along the sample thickness from the surface toward inner region using a Leica RM2245 microtome. The detailed information about sample preparation is schematically shown in Figure 1. Note that the selection of two different positions on the molded bars along flow direction is to evaluate the influence of flow strength on the molecular

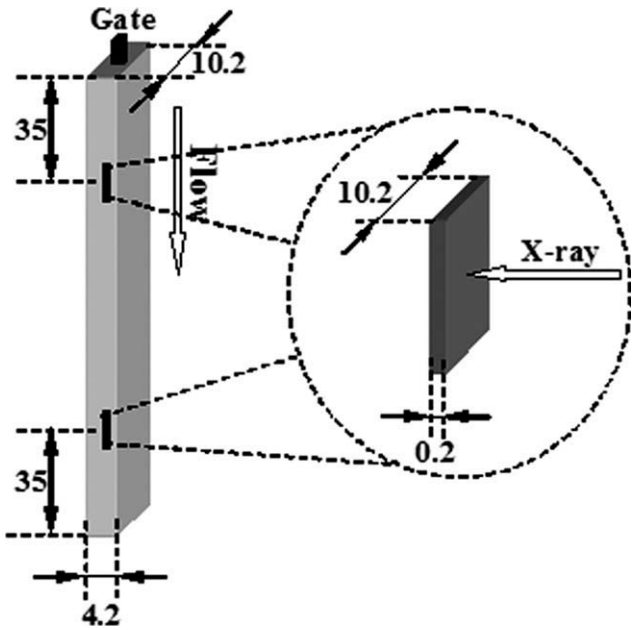

Figure 1 Schematic diagram of sample preparation for 2D-WAXD measurements.

orientation and crystal modification, as flow strength is gradually decreased along flow direction due to fountain effect during injection molding.[27,28]

For quantitative analysis of relative crystal fraction, diffraction profiles were obtained from the patterns with the subtraction of background scattering. The crystallinity of β-form was calculated from diffraction profiles using[20,29]

$$X_\beta = K_\beta \times X_c \tag{1}$$

$$K_\beta = \frac{A_\beta(300)}{A_\alpha(110) + A_\alpha(040) + A_\alpha(130) + A_\beta(300)} \tag{2}$$

$$X_c = \frac{\Sigma A_{\text{crystal}}}{\Sigma A_{\text{crystal}} + \Sigma A_{\text{amorphous}}} \tag{3}$$

where $A_{\alpha,\beta}$ (hkl) is the area of reflection peak associated with α-form or β-form, and $\Sigma A_{\text{crystal}}$ and $\Sigma A_{\text{amorphous}}$ are the areas of crystal and amorphous peaks, respectively.

Polarized optical microscopy

The hierarchical structure and crystal morphology were disclosed by a polarized optical microscope coupled with a hot stage under cross-polarization conditions. The thin slices were taken along a plane parallel to flow direction from the midwidth region of the bars, 35 mm away from the gate.

Scanning electron microscopy

The fracture morphology of the bars collected after Izod impact tests was observed by a FEI inspect

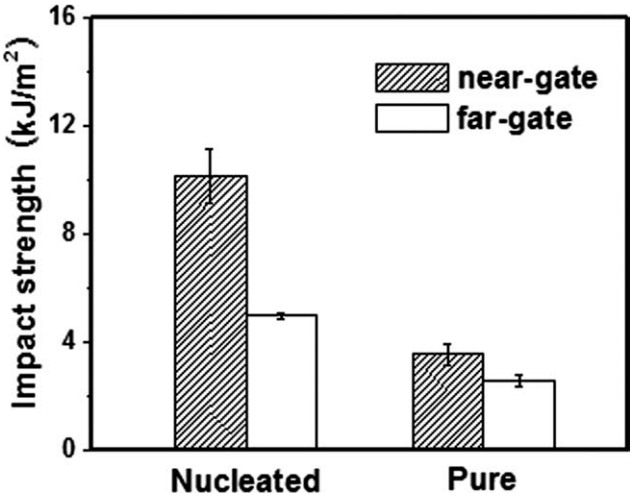

Figure 2 Evolution of notched impact strength in the nucleated and pure bars with respect to the notch location.

field emission scanning electron microscope (SEM). Before observation, the surface was sputtered by a thin gold layer.

Dynamic mechanical analysis

The modulus of molded bars were evaluated using a TA instruments Q800 dynamic mechanical analyzer (DMA) in single cantilever mode at a heating rate of 3°C/min and a frequency of 1 Hz. Allowing for the structural difference in the molded bars along flow direction, testing part was nearly located at 35 mm away from two ends, respectively.

Notched impact tests

The toughness of notched bars was determined by an Izod impact tester at room temperature. Before impact tests, a 2-mm V-shaped notch, located at 35 mm away from two ends, respectively, was introduced along the sample width. For convenience, the bars with notches near and far from the gate were designated as near-gate and far-gate, respectively. All bars were stored at room temperature for 1 day before notching, and the Izod impact tests were conducted the following day after the samples were notched. For each sample, the reported toughness was averaged over six specimens.

RESULTS AND DISCUSSION

Figure 2 depicts the impact strength of β-nucleated and pure iPP bars with different notch location away from the gate. It is indicated that incorporation of β-nucleating agent in iPP is beneficial for toughness enhancement, regardless of notch location. At the same time, notch location also has dramatic influence on the toughness of both β-nucleated and pure iPP samples; and the specimens with notches near the gate exhibit higher toughness than those with notches far from the gate. It becomes more significant in the bars containing β-nucleating agent; about 100% increase in the toughness is achieved. Further insight into toughness enhancement from the microscopic view was gained by inspecting the fracture morphology; and corresponding SEM results are given in Figure 3. As expected, the roughness of fracture surface is exactly consistent with the toughness; the rougher is the fracture surface, the higher toughness is realized.

It is well known that melt adjacent to the wall of a cold mold undergoes rapid cooling and solidification, which, in turn, reduces the cross section of flow channel and correspondingly enhances the flow strength. The nearer is the location from the gate, the higher is the extent of solidification and thus flow strength (i.e., fountain effect).[27,28] Therefore, it can be deduced that high flow strength near the gate, in favor of molecular orientation (see below), should be responsible for the toughness improvement to some extent. Meanwhile, adding β-nucleating agent benefits further toughness improvement, while comparing the toughness of the near-gate bars

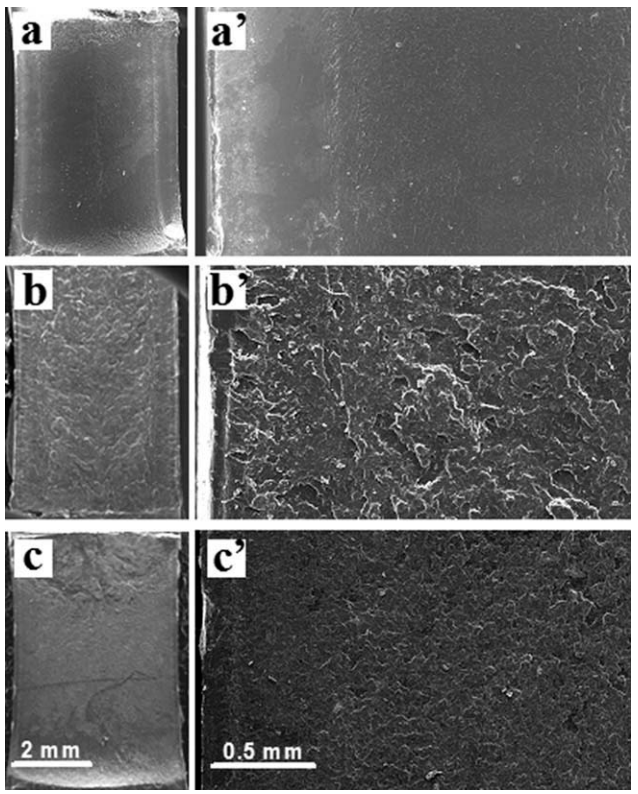

Figure 3 SEM micrographs revealing the fracture morphology along the cross section of molded bars (a–c: global view, a′–c′: enlarged view): (a and a′) pure and near-gate, (b and b′) nucleated and near-gate, and (c and c′) nucleated and far-gate. The impact direction is from up to bottom.

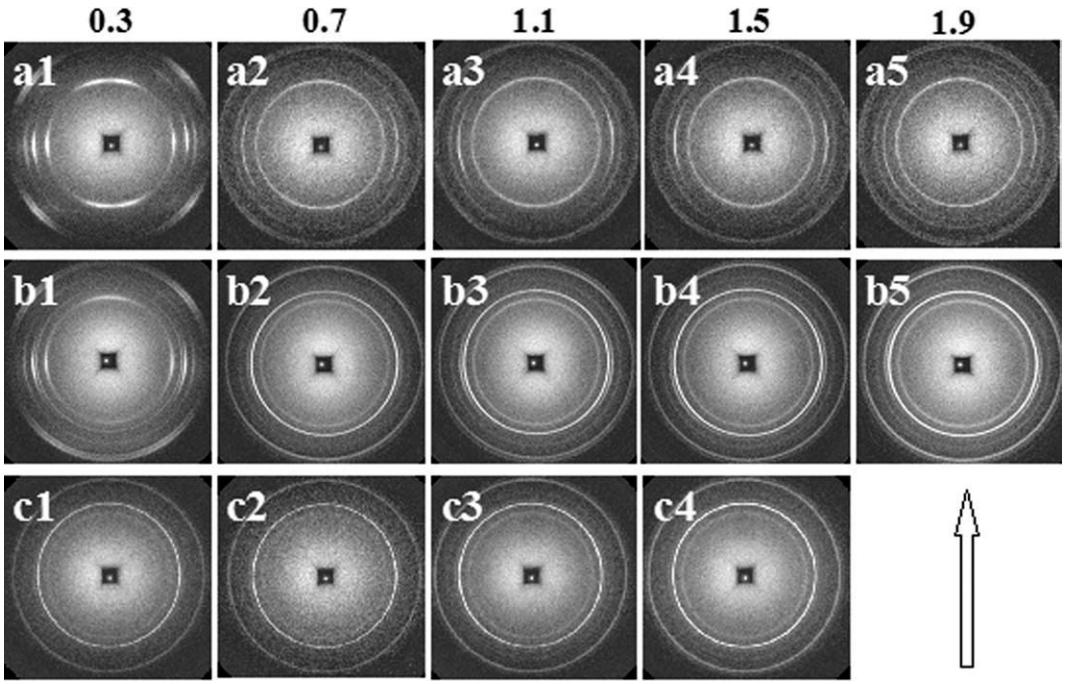

Figure 4 2D-WAXD patterns of the slices cut from the indicated depth (numbers at the top) away from the surface: (a1–a5) pure and near-gate, (b1–b5) nucleated and near-gate, and (c1–c4) nucleated and far-gate. The arrow nearly indicates the flow direction.

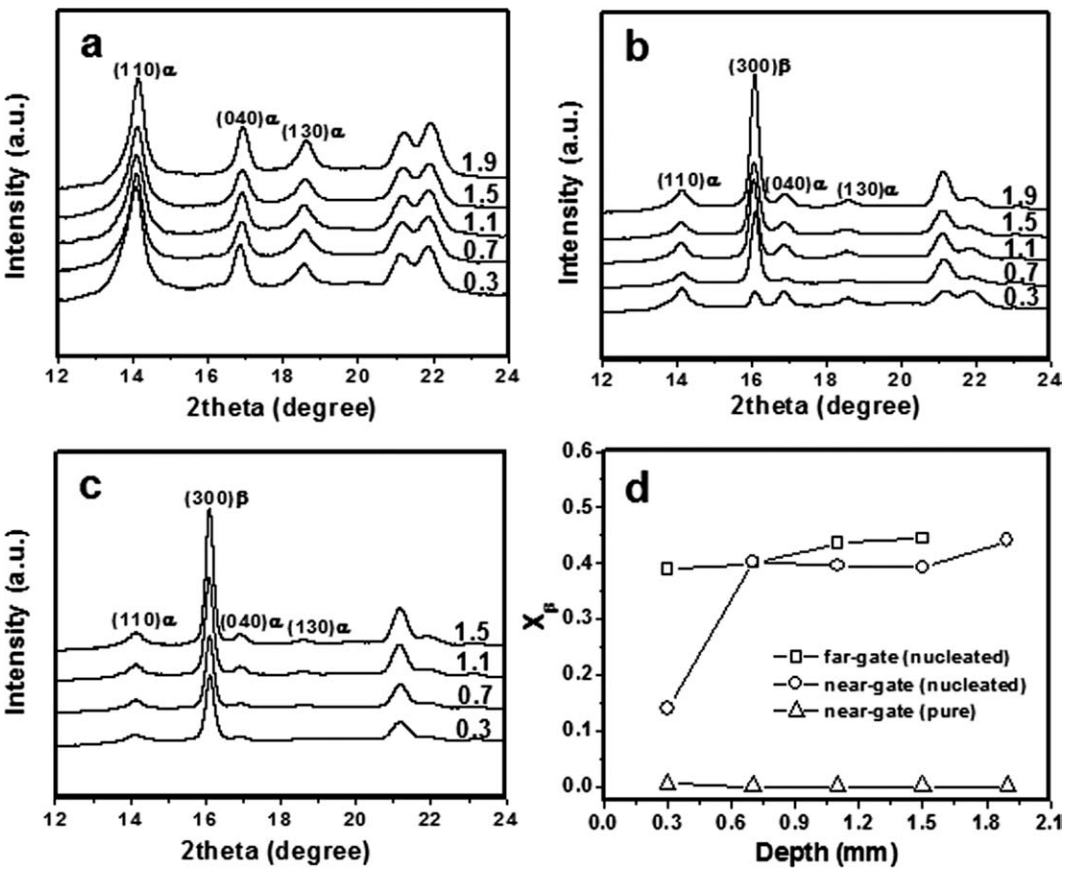

Figure 5 Depth-dependent diffraction profiles deduced from the 2D-WAXD patterns: (a) pure and near-gate, (b) nucleated and near-gate, and (c) nucleated and far-gate. The crystallinity of β-form with respect to the depth away from the surface is included in (d).

with and without β-nucleating agent. Of note, the toughness of the far-gate bars with β-nucleating agent, albeit increased, is still lower than that of β-nucleated bars near the gate. In such a sense, it suggests that combination of high flow strength and β-nucleating agent are cooperative on toughening iPP bars prepared via conventional injection molding.

Figure 4 is the 2D-WAXD patterns obtained from different depths away from the surface in the β-nucleated and pure iPP bars with respect to the distance from the gate. It is indicated that molecular orientation depends not only on the depth away from the surface but also on the distance from the gate. Of note, molecular orientation is manifested by the diffraction arcs on the patterns; and a decrease in molecular orientation corresponds to the weakening of the arcs into circles. In the near-gate bars, remarkable molecular orientation is exhibited in the region close to the surface (i.e., skin layer), irrespective of β-nucleating agent, correlating with high flow strength and flow-induced crystallization during filling stage. Toward inner region, molecular orientation becomes less apparent because of the decay of flow strength. As for the far-gate bars, however, molecular orientation is nearly absent from the surface to core region, further confirming that flow strength is decreased with the increasing distance from the gate.

On the other hand, the formation of β-form in the bars with β-nucleating agent also shows significant dependence on the flow strength, as clearly demonstrated by the deduced diffraction profiles in Figure 5. It is worthwhile to note that α-form has its reflection peaks of (110), (040), and (130) planes, whereas the reflection peak of (300) plane belongs to β-form. The formation of β-form is suppressed close to the surface especially in the nucleated bars near the gate; and the crystallinity of β-form is only about 0.15. In contrast, high fraction of β-form, manifested by the crystallinity of about 0.4, is observed toward inner part. This hierarchical distribution of β-form is further confirmed by polarized optical microscopy measurements on the nucleated bars near the gate, as shown in Figure 6. Herein, β-form is selectively melted at 150°C as regarding the difference of melting point between α-form and β-form.[30–33] From the global view, a typical hierarchical morphology is observed, including skin, intermediate, and core

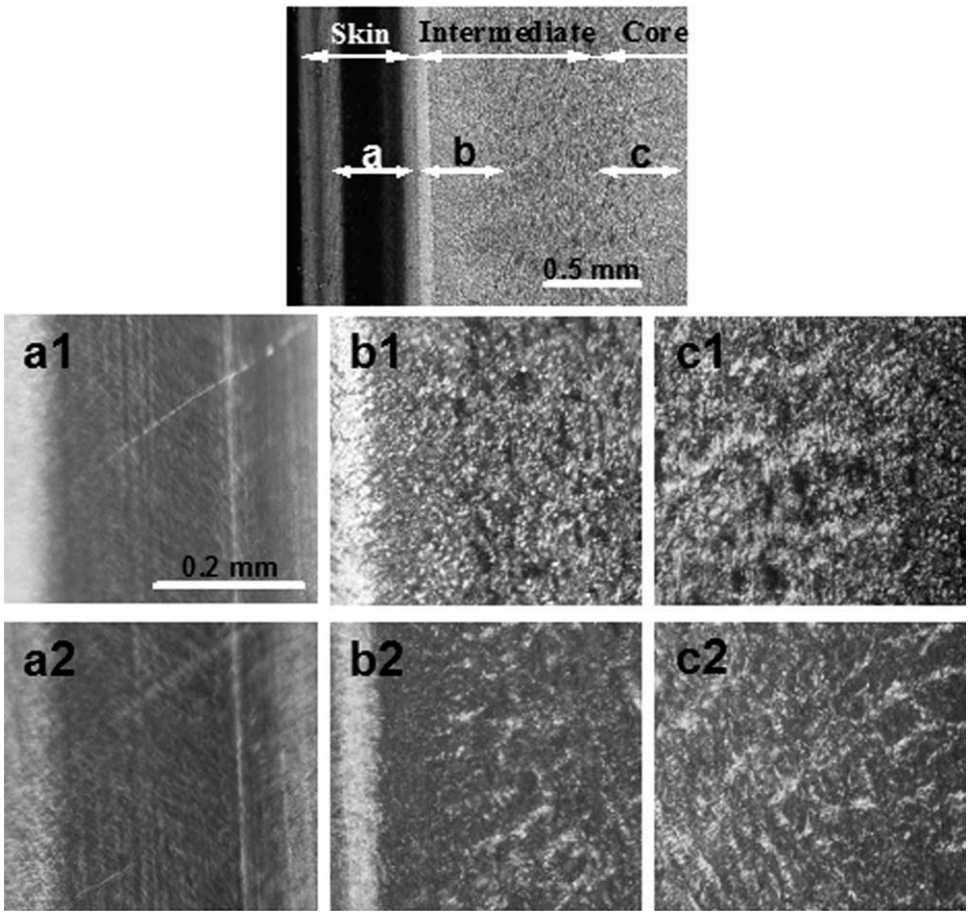

Figure 6 Polarized optical micrographs revealing hierarchical structure and distribution of β-form across the thickness in the nucleated bars near the gate: (a1–c1) before and (a2–c2) after selective melting of β-form. The flow direction is nearly vertical.

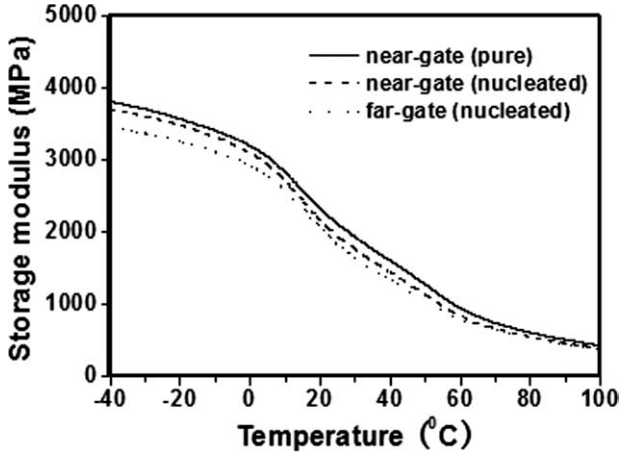

Figure 7 Change of storage modulus in the molded bars with respect to β-nucleating agent and the distance away from the gate.

layers (as labeled on the image), as a result of flow and thermal gradients during injection molding.[23–26,34] A close inspection reveals that the distribution of β-form along sample thickness is inhomogeneous; β-form is hardly discernable in the skin layer but becomes rich in the intermediate and core layers.

This variation in the fraction of β-form along the cross section of molded bars with β-nucleating agent arises from different thermal–mechanical effects endured by melt during injection molding. The melt close to the surface is cooled more rapidly than that in the core region, thus in part accounting for lower fraction of β-form in the skin layer.[35,36] On the other hand, flow strength also varies along the sample thickness and has a maximum close to the surface, i.e., in the skin layer. As demonstrated in other studies,[19–22] increasing flow strength can suppress the formation of β-form due to preferential α-nucleation induced by flow. Generation of numerous of α-nuclei favors the growth of α-crystals, and thus, the growth space for β-form induced by β-nucleating agent is limited. Moreover, while comparing the fraction of β-form in the near-gate and far-gate nucleated bars close to the surface where nearly identical cooling rate is experienced, it is highly expected that flow strength is dominant over thermal effect on the formation of β-form during injection molding.

So far, a clear picture regarding molecular orientation and β-form is gained in the conventional injection-molded bars with β-nucleating agent. In the skin layer, extensive flow suppresses the formation of β-form but favors the generation of oriented α-form. With the decay of flow strength toward inner region, an opposite tendency is exhibited in the intermediate and core layers. This hierarchical texture depends on the distance from the gate and becomes significant in the near-gate-nucleated bars enduring strong flow effect. It, in turn, is responsible for the remarkable toughness enhancement in these bars (see Fig. 2), arising from the cooperative effect of oriented α-form in the skin layer and rich β-form in the inner region. This argument is verified by the fact that neither oriented α-form in the skin layer nor rich β-form in the inner region can endow superior toughness, as demonstrated by the near-gate pure bars, nor far-gate nucleated ones. In addition, as shown by the DMA results in Figure 7, generation of oriented α-form with intrinsic rigidity in the near-gate-nucleated bars also enhance the stiffness to some extent in a wide temperature range, as compared to that of far-gate-nucleated ones with relative high fraction of ductile β-form.[37,38]

CONCLUSIONS

This study clearly demonstrates that superior toughness can be achieved in the conventional injection-molded iPP parts through the combined effect of flow and β-nucleating agent. With detailed structural analysis across the thickness of hierarchical bars, this superior toughness arises from the cooperative effect of oriented α-form induced by extensive flow in the skin layer and rich β-form generated by β-nucleating agent in the inner region. Neither oriented α-form in the skin layer nor rich β-form in the inner region can result in such superior toughness, albeit some extent of toughness improvement. Our finding may pave a path to achieve high performance of iPP by tailoring hierarchical molecular orientation and crystal modification in practical processing.

References

1. Haeringen, D. T. V.; Varga, J.; Ehrenstein, G. W.; Vancso, G. J. J Polym Sci Polym Phys 2000, 38, 672.
2. Li, J. X.; Cheung, W. L. Polymer 1998, 39, 6935.
3. Li, J. X.; Cheung, W. L.; Chan, C. M. Polymer 1999, 40, 2089.
4. Chu, F.; Kimura, Y. Polymer 1996, 37, 573.
5. Romankiewicz, A.; Jurga, J.; Sterzynski, T. Macromol Symp 2003, 202, 281.
6. Zhang, Z.; Tao, Y.; Yang, Z.; Mai, K. Eur Polym J 2008, 44, 1955.
7. Varga, J.; Ehrenstein, G. W. Polymer 1996, 31, 5959.
8. Ščudla, J.; Raab, M.; Eichhorn, K. J.; Strachota, A. Polymer 2003, 44, 4655.
9. Bai, H.; Wang, Y.; Zhang, Z.; Han, L.; Li, Y.; Liu, L.; Zhou, Z.; Men, Y. Macromolecules 2009, 42, 6647.
10. Luo, F.; Geng, C.; Wang, K.; Deng, H.; Chen, F.; Fu, Q.; Na, B. Macromolecules 2009, 42, 9325.
11. Yamamoto, Y.; Inoue, Y.; Onai, T.; Doshu, C.; Takahashi, H.; Uehara, H. Macromolecules 2007, 40, 2745.
12. Lovinger, A. J.; Chua, J. O.; Gryte, C. C. J Polym Sci Polym Phys Ed 1977, 15, 641.
13. Varga, J.; Karger-Kocsis, J. J Polym Sci Polym Phys 1996, 34, 657.
14. Somani, R. H.; Hsiao, B. S.; Nogales, A.; Fruitwala, H.; Srinivas, S.; Tsou, A. H. Macromolecules 2001, 34, 5902.
15. Zhang, C. G.; Hu, H. Q.; Wang, D. J.; Yan, S.; Han, C. C. Polymer 2005, 46, 8157.

16. Dong, M.; Gou, Z. X.; Yu, J.; Su, Z. Q. J Polym Sci Polym Phys 2008, 46, 1725.
17. Varga, J.; Menyhárd, A. Macromolecules 2007, 40, 2422.
18. Chvatalova, L.; Navratilova, J.; Cermak, R.; Raab, M.; Obadal, M. Macromolecules 2009, 42, 7413.
19. Chen, Y. H.; Mao, Y. M.; Li, Z. M.; Hsiao, B. S. Macromolecules 2010, 43, 6760.
20. Huo, H.; Jiang, S.; An, L. Macromolecules 2004, 37, 2478.
21. Su, R.; Zhang, Z.; Gao, X.; Ge, Y.; Wang, K.; Fu, Q. J Phys Chem B 2010, 114, 9994.
22. Chen, Y. H.; Zhong, G. J.; Wang, Y.; Li, Z. M.; Li, L. Macromolecules 2009, 42, 4343.
23. Kantz, M. R.; Newman, H. D.; Stigale, F. H., Jr. J Appl Polym Sci 1972, 16, 1249.
24. Martin, J.; Margueron, S.; Fontana, M.; Cochez, M.; Bourson, P. Polym Eng Sci 2010, 50, 138.
25. Mendoza, R.; Régnier, G.; Seiler, W.; Lebrun, J. L. Polymer 2003, 44, 3363.
26. Zhu, P. W.; Edward, G. Polymer 2004, 45, 2603.
27. Tadmor, Z. J Appl Polym Sci 1974, 18, 1753.
28. Mavridis, H.; Hrymak, A. N.; Vlachopoulos, J Polym Eng Sci 1986, 26, 449.
29. Turner Jones, A.; Cobbold, A. J. J Polym Sci Polym Lett 1968, 6, 539.
30. Ščudla, J.; Eichhorn, K. J.; Raab, M.; Schmidt, P.; Jehnichen, D.; Häußler, L. Macromol Symp 2002, 184, 371.
31. Vleeshouwers, S. Polymer 1997, 38, 3213.
32. Zhou, J.; Li, L.; Lu, J. Polymer 2006, 47, 261.
33. Cho, K.; Saheb, D. N.; Choi, J.; Yang, H. Polymer 2002, 43, 1407.
34. Zhu, P. W.; Edward, G. J Mater Sci 2008, 43, 6459.
35. Na, B.; Lv, R.; Xu, W.; Chen, R.; Zhao, Z.; Yi, Y. Polym Int 2008, 57, 1128.
36. Marco, C.; Gómez, M. A.; Ellis, G.; Arribas, J. M. J Appl Polym Sci 2002, 86, 531.
37. Castelein, G.; Coulon, G.; G'sell, C.; Nancy, E. Polym Eng Sci 1997, 37, 1694.
38. Lezak, E.; Bartczak, Z.; Galeski, A. Polymer 2006, 47, 8562.